Effects of a variable frequency drive on torsional vibrations in electrical machines

Hannu Hartikainen

School of Electrical Engineering

Thesis submitted for examination for the degree of Master of Science in Technology.

Espoo 30.12.2022

Supervisor

Prof. Marko Hinkkanen

Advisor

Sampo Laine, M.Sc.(Tech.)

Aalto University
School of Electrical
Engineering

Aalto University
School of Electrical
Engineering

Aalto University, P.O. BOX 11000, 00076 AALTO
www.aalto.fi
Abstract of the master's thesis

Author Hannu Hartikainen

Title Effects of a variable frequency drive on torsional vibrations in electrical machines

Degree programme Automation and Electrical Engineering

Major Electrical Power and Energy Engineering **Code of major** ELEC3024

Supervisor Prof. Marko Hinkkanen

Advisor Sampo Laine, M.Sc.(Tech.)

Date 30.12.2022 **Number of pages** 30 **Language** English

Abstract

This thesis deals with the identification of electromagnetic stiffness and damping. It is well known that electromagnetic stiffness and damping influence the torsional dynamics of an electric drivetrain. The electromagnetic stiffness and damping are obtained from a frequency response between the rotor angle and the electromagnetic torque, which could be identified or calculated analytically. However, the frequency response is usually only for a machine directly connected to the grid and does not include the effect of a variable frequency drive. The variable frequency drive is a common way to control the speed and torque of the machine. The main goal of this thesis is to develop a method that includes the effect of the variable frequency drive control on the frequency response. The identification method is based on a signal injection in time-domain simulations. The simulation model includes a discrete-time controller and a continuous-time motor model. In the simulation, an excitation signal is injected into the steady-state rotor speed, where the response is seen in the electromagnetic torque. The frequency response could be identified with the rotor speed and the electromagnetic torque spectra. The identification method is validated with analytical solutions of the frequency response from the literature. The validation includes one machine with three control methods for the variable frequency drive.

Keywords Damping, electromagnetic, electric machine, frequency response, identification, stiffness, torsional vibration, variable frequency drive

Aalto University
School of Electrical
Engineering

Aalto-yliopisto, PL 11000, 00076 AALTO
www.aalto.fi
Diplomityön tiivistelmä

Tekijä Hannu Hartikainen

Työn nimi Taajuusmuuttajan vaikutus sähkökoneiden vääntövärähtelyhin

Koulutusohjelma Automaatio ja sähkötekniikka

Pääaine Sähköenergiatekniikka **Pääaineen koodi** ELEC3024

Työn valvoja Prof. Marko Hinkkanen

Työn ohjaaja Sampo Laine, dipl.ins.

Päivämäärä 30.12.2022 **Sivumäärä** 30 **Kieli** Englanti

Tiivistelmä

Tämä diplomityö käsittelee sähkömagneettisen jäykkyyden ja vaimennuksen identifiointia. Sähkömagneettinen jäykkyys ja vaimennus vaikuttaa sähköisen voimalinjan vääntödynamiikkaan. Sähkömagneettinen jäykkyys ja vaimennus voidaan laskea roottorin kulman ja sähkömagneettisen vääntömomentin välisestä taajuusvasteesta. Usein taajusvasteessa ei oteta huomioon taajuusmuuttajan säätömenetelmää. Taajuusmuuttajalla voidaan ohjata sähkökoneen tuottamaa vääntömomenttia, sekä pyörimisnopeutta. Työn päätavoite on kehittää menetelmä, jonka avulla voidaan identifioida taajuusvaste ohjatulle sähkökoneelle. Menetelmä perustuu aikatason simulointeihin, joissa injektoidaan herätettä roottorin pysyvän tilan pyörimisnopeuteen. Heräte on havaittavissa sähkökoneen tuottamassa vääntömomentissa, jolloin taajuusvaste on laskettivassa roottorin pyörimisnopeuden ja vääntömomentin spektreistä. Simulaatiomallissa on diskreetiaikainen säätömenetelmä ja jatkuvan ajan sähkökonemalli. Menetelmä validoidaan vertaamalla identifioituja taajuusvasteita analyyttisesti laskettuihin taajusvasteisiin.

Avainsanat Identifiointi, jäykkyys, sähkökone, sähkömagneettinen, taajuusmuuttaja, taajuusvaste, vaimennus, vääntövärähtely

Preface

I would like to thank my supervisor Prof. Marko Hinkkanen and my instructor Sampo Laine for their valuable comments regarding the topic and guidance in scientific writing. Working with this multidisciplinary research topic that combines electrical and mechanical engineering was an absolute pleasure. I would also like to thank the Electric Drives Group for their support.

Otaniemi, 30.12.2022

Hannu Hartikainen

Contents

Symbols and abbreviations

Notation

Hat is used to indicate estimated value, e.g., $\hat{\boldsymbol{\psi}}_{\mathrm{R}}$.
Tilde is used to indicate estimation error, e.g., $\tilde{\boldsymbol{\psi}}_{\mathrm{R}}$.
Subscript 0 is used to indicate steady-state value, e.g., $\boldsymbol{\psi}_{\mathrm{R0}}$.

Latin symbols

$\mathbf{0}$	Zero matrix
$\boldsymbol{A}$	State matrix
$\boldsymbol{A}_{\mathrm{cc}}$, $\boldsymbol{A}_{\mathrm{co}}$	Closed-loop state matrices
$\boldsymbol{B}_{\mathrm{s}}$, $\boldsymbol{b}_{\mathrm{s}}$, $\boldsymbol{b}_{\mathrm{m}}$	Input matrices
c_{e}	Electromagnetic damping
$\boldsymbol{C}$, $\boldsymbol{c}_{\mathrm{m}}$, $\boldsymbol{C}_{\mathrm{s}}$	Output matrices
$\boldsymbol{C}(s)$	Compensator
$\boldsymbol{e}$	Correction vector
f_{n}	Motor nominal frequency
$G_\theta(\mathrm{j}\omega)$, $G_\omega(\mathrm{j}\omega)$	Frequency response
$G(s)$, $G_{\mathrm{c}}(s)$, $G_{\mathrm{co}}(s)$, $G_{\mathrm{o}}(s)$	Transfer function
$\mathbf{I}$	Identity matrix
$\boldsymbol{i}_{\mathrm{abc}}$	Stator phase current column vector
I_{M}	Rotor inertia
$\boldsymbol{i}^{\mathrm{s}}_{\mathrm{m}}$, $\boldsymbol{i}^{\mathrm{s}}_{\mathrm{M}}$	Magnetizing current vector
$\boldsymbol{i}^{\mathrm{s}}_{\mathrm{r}}$, $\boldsymbol{i}_{\mathrm{r}}$, $\boldsymbol{i}^{\mathrm{s}}_{\mathrm{R}}$	Rotor current vectors
$\boldsymbol{i}_{\mathrm{sf}}$	Low-pass filtered stator current
$\boldsymbol{i}^{\mathrm{s}}_{\mathrm{s}}$, $\boldsymbol{i}_{\mathrm{s}}$	Stator current vectors
$\boldsymbol{i}_{\mathrm{s,ref}}$	Stator current reference vectors
$\mathbf{J}$	Orthogonal rotation matrix
$\boldsymbol{K}$, $\boldsymbol{K}_{\mathrm{c}}$, $\boldsymbol{K}_{\mathrm{o}}$	Gain matrices
k_{e}	Electromagnetic stiffness
k_{u}, k_ω	Gain parameters
$\boldsymbol{k}^{\mathrm{T}}$	Gain vector
L_{m}, L_{M}	Magnetizing inductances
L_{r}, $L_{\mathrm{r}\sigma}$	Rotor inductances
L_{s}, $L_{\mathrm{s}\sigma}$, L_σ	Stator inductances
p	Motor pole pairs
R_{r}, R_{R}	Rotor resistances
R_{s}	Stator resistance
R_σ	Total resistance
s	Laplace variable
$\boldsymbol{u}^{\mathrm{s}}_{\mathrm{s}}$, $\boldsymbol{u}_{\mathrm{s}}$	Stator voltage vectors
$\boldsymbol{u}_{\mathrm{s,ref}}$	Stator voltage reference vector
$\boldsymbol{x}$	State vector

Greek symbols

α	Inverse rotor time constant
α_f	Filter bandwidth
$\boldsymbol{\psi}_\mathrm{r}^\mathrm{s}$, $\boldsymbol{\psi}_\mathrm{R}^\mathrm{s}$, $\boldsymbol{\psi}_\mathrm{R}$	Rotor flux linkage vectors
$\boldsymbol{\psi}_\mathrm{s}^\mathrm{s}$, $\boldsymbol{\psi}_\mathrm{s}$	Stator flux linkage vectors
τ_m	Electromagnetic torque
ω_m, ω_M	Rotor angular frequencies
ω_r	Slip angular frequency
ω_rb	Breakdown slip frequency
ω_s	Stator angular frequency
$\omega_\mathrm{s,ref}$	Stator reference angular frequency

Operators

$\dfrac{\mathrm{d}}{\mathrm{d}t}$	derivative with respect to variable t
$\int$	Integral
sin(), cos()	Sine and cosine functions
T	Transpose
Δ	Small-signal quantity

Abbreviations

DC	direct current
VFD	Variable frequency drive
V/Hz	Volts-per-hertz

1 Introduction

More than half of the electricity is consumed in systems driven by electric motors globally [1]. In practice, the electrical motor is always connected to a mechanical system, which could be a fan, a pump, etc. Typically, the flow rate needs to be controlled in pumps. A simple way is to use a valve, but this will affect the system efficiency. Another method is to use, a variable frequency drive (VFD) which is becoming more popular in electric motors for a variety of reasons, including potential energy savings and controllability of the system. The VFD controls the motor speed by changing the voltage and frequency supplied to the motor.

The pump could be seen as a simple two-mass lumped-element system, where the load and the rotor are modeled as the masses connected with a shaft. Whenever there is torque applied to the system, the shaft will have some torsion, and often it will also experience torsional vibration, i.e. twisting motion of the shaft about its own axis [2]. Typically, only rotor inertia is included in a torsional analysis, but it is well known that an electromagnetic torque will affect the torsional vibration [3–7]. One way to include the effect of the motor in the torsional analysis is to use electromagnetic stiffness and damping obtained from the frequency response between rotor angle and electromagnetic torque [7].

The VFD controls the electromagnetic torque and the speed of the motor. Hence, the electromagnetic stiffness and damping should be affected by the VFD when controlling the motor. There are many ways to control the voltage and frequency, ranging from simple and low-performance open-loop volts-per-hertz (V/Hz) control to complex and high-performance control, such as field-oriented control and direct torque control. It is known that an operating point and the control method affect the stability of the motor [8–10].

The problem with the torsional analysis for electric drivetrains is that the analysis rarely includes the motor model. Even if the motor model is included, the effect of the VFD control is not taken into account which is essential for calculating the correct electromagnetic stiffness and damping. A few analytical solutions exist that include the control of the VFD [9, 10]. However, the analytical models are nearly impossible to formulate for complex control methods. Furthermore, control methods are not publicly shared since it is a trade secrets for the manufacturers. Therefore, manufacturers should be able to give a black-box model without revealing the control method. In the current literature, there is no suitable method to include the VFD effects in electromagnetic stiffness and damping, especially if the control scheme is advanced.

This thesis aims to develop a method to identify the controlled motor frequency response from the rotor angle to the electromagnetic torque at different operating conditions from time-domain simulations. In particular, the thesis aims to answer the following question: Can a frequency response function from the rotor angle to the electromagnetic torque be obtained from time-domain simulations? The identification will be done with a small-signal injection around the steady-state operating point. Simulations will utilize continuous-time dynamic motor models and discrete-time control algorithms. Furthermore, identified frequency responses will be compared to

known analytical models from the literature [9, 10].

The scope of this thesis will be limited to simulations. In these simulations, induction motor is used which is controlled with V/Hz and observer-based V/Hz [9,10]. The outcome of the thesis is validation that the frequency response can be obtained from time-domain simulations.

This thesis proposes a time-domain simulation-based identification method for obtaining the frequency response from motor angle to electromagnetic torque. In this method, the controller could be a black box in the simulations. The electromagnetic stiffness and damping for torsional analysis could be calculated using the frequency response.

The rest of the thesis is divided into four chapters. Chapter 2 presents electromagnetic stiffness and damping and proposes a method to obtain the frequency response for the stiffness and damping. Chapter 3 shows the motor model, control method, and derived analytical small-signal models for the verification. Chapter 4 describes the implementation of the identification algorithm in an open source *motulator* motor drive simulator and compares the analytical and identified frequency responses. Lastly, Chapter 5 concludes the thesis and suggests future work.

2 System identification

The system identification of electromagnetic stiffness and damping is based on time-domain simulation. The electromagnetic stiffness and how it is obtained are introduced in section 2.2, and then the identification method is shown in section 2.3

2.1 Frequency response

A frequency response contains phase shift and amplification between input and output as a function of frequency. At each frequency, the frequency response is a complex quantity, represented either with real and imaginary parts or in polar form. A transfer function and frequency response are closely related to each other. The transfer function is

$$G(s) = \frac{Y(s)}{U(s)} \tag{1}$$

where $U(s)$ is input, $Y(s)$ is output, and s is the Laplace variable. Furthermore, the frequency response is obtained by substituting $s = \mathrm{j}\omega$ into the transfer function [11].

The frequency response describes a linear time-invariant system response to a sinusoidal input. When the system is excited with

$$u(t) = u_{\text{amp}} \sin(\omega t + \alpha) \tag{2}$$

where u_{amp} is amplitude, ω is angular frequency, and α is phase shift. Then in the steady state, the output contains the same frequency sinusoid, as

$$y(t) = y_{\text{amp}} \sin(\omega t + \beta) \tag{3}$$

where y_{amp} is amplitude and β is phase shift [12]. The magnitude for the frequency response at angular frequency ω is obtained as

$$|G(\mathrm{j}\omega)| = \frac{y_{\text{amp}}}{u_{\text{amp}}}. \tag{4}$$

The angle as

$$\angle G(\mathrm{j}\omega) = \beta - \alpha. \tag{5}$$

The input and output could be shown in phasor form, where the resulting frequency response is [12]

$$G(\mathrm{j}\omega) = \frac{Y(\omega)}{U(\omega)}. \tag{6}$$

2.2 Equivalent torsional stiffness and damping

An equivalent torsional stiffness and damping are usually associated with the mechanical components of a drivetrain. The stiffness could be thought of as a spring that stores energy when compressed, but instead of compression, it is a torsion along the shaft shown in Figure 1. The angle θ depends on the stiffness of the shaft and the torque τ that is applied to the shaft. This torsion occurs whenever a torque is

transmitted. The damping dissipates the energy in torsional vibrations, but often the shaft that transmits the torque has low damping.

Torsional vibration is a twisting motion of the shaft about its own axis [2]. In the ideal case, the angle of the twist stays constant in the steady state. Then there would be just constant torque over the shaft. But in reality, the load and torque production are not constant in rotating machines. There are always some changes in torque that act as an excitation for torsional vibrations. These torsional vibrations are hard to detect without specialized measurement equipment [2].

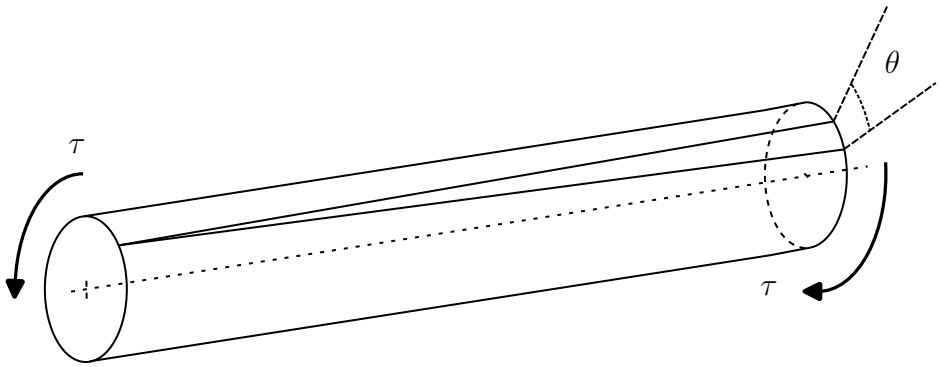

Figure 1: Torsion in a shaft, where τ is torque and θ is angle of twist.

A two-mass lumped-element model, as shown in Figure 2, is one simplified method to model a system with an electric motor and load. The model has a stator, a rotor, and a load. The stator is the ground for the model and the rotor is connected to it with an electromagnetic stiffness k_e and damping c_e. The rotor and the load are connected with a massless shaft that has stiffness k and damping c.

In torsional analysis commonly the electromagnetic stiffness and damping between stator and rotor are omitted, and only the rotor inertia I_M is included. One of the earliest inclusions of electromagnetic interaction in the torsional analysis was done with directly online connected synchronous machines and an electrical grid [4, 5]. It was shown that the electrical grid had a major effect on electromagnetic stiffness and damping. The method used synchronizing torque and damping torque from the electromagnetic stiffness and damping were calculated. Furthermore, the electromagnetic stiffness and damping were summed with mechanical stiffness and damping. The method was called a complex torque coefficient. This complex torque method was proven insufficient for the torsional analysis [6].

It is well known that the electromagnetic stiffness k_e and damping c_e affect the torsional characteristics, especially in the first few torsional modes, and it could be included in the torsional analysis [13, 14]. The electromagnetic stiffness and damping depend on the motor parameters and operating point [7]. The electromagnetic stiffness and damping are obtained from a frequency response

$$G_\theta(\mathrm{j}\omega) = \frac{\Delta\tau_\mathrm{m}(\omega)}{\Delta\theta_\mathrm{m}(\omega)} \tag{7}$$

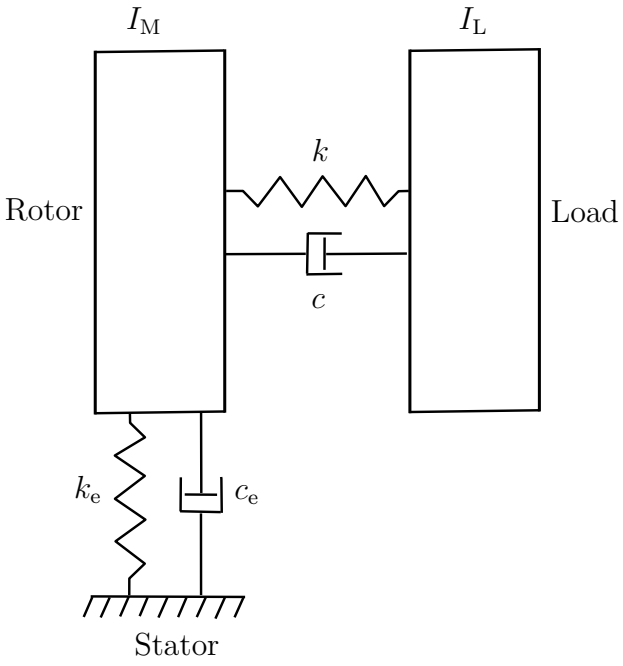

Figure 2: Two-mass model with electromagnetic stiffness k_e and damping c_e between stator and rotor.

where $\Delta\tau_\mathrm{m}$ is a small-signal electromagnetic torque and $\Delta\theta_\mathrm{m}$ is a small-signal rotor angle. The small-signal values are used since equivalent stiffness and damping are based on linearized models. Where the twist of the shaft angle occurs around the equilibrium point. Furthermore, the electromagnetic stiffness and damping are obtained from the frequency response (7) as [7]

$$k_\mathrm{e}(\mathrm{j}\omega) = -\mathrm{Re}\{G_\theta(\mathrm{j}\omega)\} \tag{8a}$$
$$c_\mathrm{e}(\mathrm{j}\omega) = -\mathrm{Im}\{G_\theta(\mathrm{j}\omega)\}/(\omega). \tag{8b}$$

2.3 Signal injection

A signal injection in the time-domain simulation is one way to identify the frequency response for the electromagnetic stiffness and damping [7]. The excitation could be injected into the rotor angle θ_m or angular frequency ω_m since the angular frequency is derivative of the angle. Then the response could be seen in the produced electromagnetic torque τ_m.

The controlled motor consists of three systems shown in Figure 3; controller, electrical subsystem, and mechanical subsystem. The electromagnetic stiffness and damping that needs to be identified are produced in the electrical subsystem, which is affected by the controller. In Figure 3, the gray background highlights the system in which frequency response $G(\mathrm{j}\omega)$ needs to be identified.

The mechanical subsystem is not required for identification, it could be removed. Figure 4 illustrates a block diagram of the simulation model where the mechanical

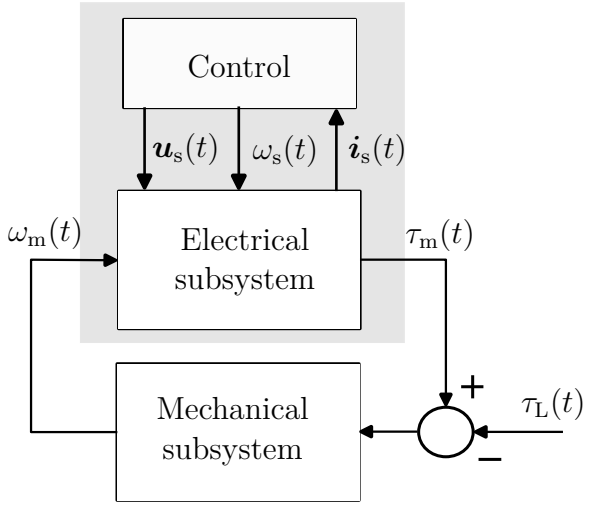

Figure 3: Large-signal block diagram of the controlled motor, where $\boldsymbol{u}_\mathrm{s}$ is the stator voltage, ω_s the stator angular frequency, $\boldsymbol{i}_\mathrm{s}$ is the stator current, and τ_L is load torque.

system is removed. Instead of the mechanical subsystem, there is an input for the motor angular frequency ω_m and an output for the electromagnetic torque τ_m. The input is determined by a desired steady-state rotor angular frequency ω_m0 and the excitation signal $\Delta\omega_\mathrm{m}$, and the output has some steady-state electromagnetic torque τ_m0 with response torque $\Delta\tau_\mathrm{m}$ from the excitation. Furthermore, the excitation signal could be a transient, a sinusoid, or a binary sequence. Each of these signals have some benefits and drawbacks.

The transient is a sudden change in the input. With the transient, the frequency response is fast to acquire since it could be done once for each operating point. The problem with this method is the signal-to-noise ratio, the change in $\Delta\omega_\mathrm{m}$ should be high enough to be noticeable, but low enough to stay in a small signal region [11]. The binary sequence is a periodic signal with two values $+A$ and $-A$ where A is the amplitude of the signal. There are multiple different versions of the binary sequence, such as a pseudo-random binary sequence and a maximum length binary sequence [15].

The sinusoid signal injection is used in the proposed identification method. The benefit is the signal-to-noise ratio is high, even when the amplitude of excitation is low. However, the big drawback of this method is the fact one simulation corresponds to one excitation frequency. This increases the simulation time to obtain the frequency response.

The signal injection is done in time-domain simulations. The time-domain input and output data are transferred to the frequency domain with the discrete Fourier transform. The transformation is carried out as

$$\Delta\omega_{\mathrm{m,DFT}}(k) = \frac{1}{N}\sum_{n=0}^{N-1}\Delta\omega_\mathrm{m}(n)\mathrm{e}^{-\mathrm{j}2\pi nk/N} \tag{9}$$

where $\Delta\omega_{\mathrm{m,DFT}}(k)$ is a kth frequency component, $\Delta\omega_\mathrm{m}(n)$ is nth sample, and N is

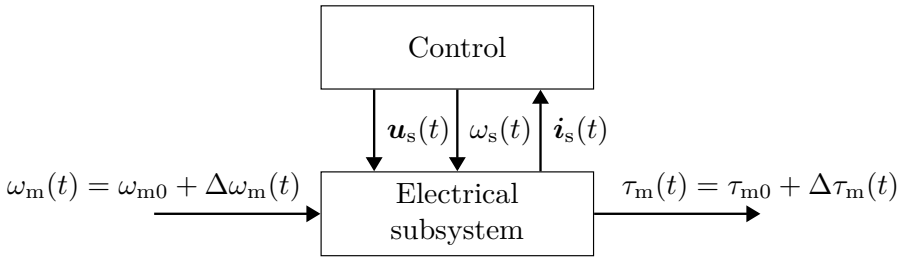

Figure 4: Block diagram of the simulation model for the identification.

the number of samples. The same transformation is carried out for $\Delta\tau_\mathrm{m}$ as well [16]. Since the identification is done with the signal injection at the steady-state operating point. The steady-state operating point has to be subtracted from the input and output data. The maximum detectable frequency is determined with the Nyquist frequency. The angular frequency for the kth value is calculated as [16]

$$\omega = \frac{2\pi k}{N}. \tag{10}$$

After frequency spectra from the electromagnetic torque and the motor speed are obtained, the frequency response is calculated as

$$G_\theta(\mathrm{j}\omega) = \frac{\Delta\tau_\mathrm{m}(\omega)}{\Delta\omega_\mathrm{m}(\omega)/\mathrm{j}\omega} = \frac{\Delta\tau_\mathrm{m}(\omega)}{\Delta\theta_\mathrm{m}(\omega)}. \tag{11}$$

From the frequency response, the electromagnetic stiffness and damping could be calculated (8). In this thesis, the frequency response is presented from the angular speed ω_m to the electromagnetic torque τ_m as

$$G_\omega(\mathrm{j}\omega) = \frac{\Delta\tau_\mathrm{m}(\omega)}{\Delta\omega_\mathrm{m}(\omega)}. \tag{12}$$

3 Motor models and control methods

The rotation speed of an asynchronous motor is affected by the load torque. The mechanical motor speed ω_M is calculated as

$$\omega_\mathrm{M} = \frac{\omega_\mathrm{m}}{p} \tag{13}$$

where p is the number of pole pairs in the motor. The electrical angular speed is

$$\omega_\mathrm{m} = \omega_\mathrm{s} - \omega_\mathrm{r} \tag{14}$$

where ω_s is the stator angular frequency and ω_r is the slip angular frequency caused by the load torque. This means that, if the motor speed needs to be controlled there are three options: the stator angular frequency ω_s, the load torque, and pole pairs p. One solution for the control is to use VFD. The VFD controls motor speed, by changing the stator angular frequency ω_s and stator voltage $\boldsymbol{u}_\mathrm{s}$.

3.1 Large-signal motor model

The motor model uses space vectors to present the voltage, current, and flux linkages. These space vectors represent three-phase quantities with two values without losing any information [17]. When the system is a balanced three-phase system the zero sequence disappears. An induction machine is one example that does not have zero-sequence because the neutral wire is not connected, and the phase currents sum up to zero. Transformations can be done with matrix multiplication

$$\boldsymbol{i}_\mathrm{s}^\mathrm{s} = \begin{bmatrix} i_\alpha \\ i_\beta \end{bmatrix} = \frac{2}{3}\begin{bmatrix} 1 & -\frac{1}{2} & -\frac{1}{2} \\ 0 & \frac{\sqrt{3}}{2} & -\frac{\sqrt{3}}{2} \end{bmatrix}\begin{bmatrix} i_\mathrm{a} \\ i_\mathrm{b} \\ i_\mathrm{c} \end{bmatrix}, \quad \boldsymbol{i}_\mathrm{abc} = \begin{bmatrix} i_\mathrm{a} \\ i_\mathrm{b} \\ i_\mathrm{c} \end{bmatrix} = \begin{bmatrix} 1 & 0 \\ -\frac{1}{2} & \frac{\sqrt{3}}{2} \\ -\frac{1}{2} & -\frac{\sqrt{3}}{2} \end{bmatrix}\begin{bmatrix} i_\alpha \\ i_\beta \end{bmatrix} \tag{15}$$

where $\boldsymbol{i}_\mathrm{s}^\mathrm{s}$ is the stator current vector in stator coordinates with $\alpha - \beta$ components and $\boldsymbol{i}_\mathrm{abc}$ is a vector with instantaneous phase current values as components. The relationship between $\alpha - \beta$ space vector and phase quantities is shown in Figure 5. Dashed lines are phase current positive directions, and the solid colored lines are instantaneous phase current vectors.

The space vector can be transferred to any arbitrarily rotating reference frame with Park transformation

$$\begin{aligned} \boldsymbol{i}_\mathrm{s}^\mathrm{a} &= \begin{bmatrix} i_\mathrm{d} \\ i_\mathrm{q} \end{bmatrix} = \begin{bmatrix} \cos(\theta_\mathrm{a}) & \sin(\theta_\mathrm{a}) \\ -\sin(\theta_\mathrm{a}) & \cos(\theta_\mathrm{a}) \end{bmatrix}\begin{bmatrix} i_\alpha \\ i_\beta \end{bmatrix} \\ \boldsymbol{i}_\mathrm{s}^\mathrm{s} &= \begin{bmatrix} i_\alpha \\ i_\beta \end{bmatrix} = \begin{bmatrix} \cos(\theta_\mathrm{a}) & -\sin(\theta_\mathrm{a}) \\ \sin(\theta_\mathrm{a}) & \cos(\theta_\mathrm{a}) \end{bmatrix}\begin{bmatrix} i_\mathrm{d} \\ i_\mathrm{q} \end{bmatrix} \end{aligned} \tag{16}$$

where θ_a is the instantaneous angle of the reference frame and a refers to the reference frame. The angle θ_a is calculated as

$$\theta_\mathrm{a} = \int \omega_\mathrm{a} \mathrm{d}t \tag{17}$$

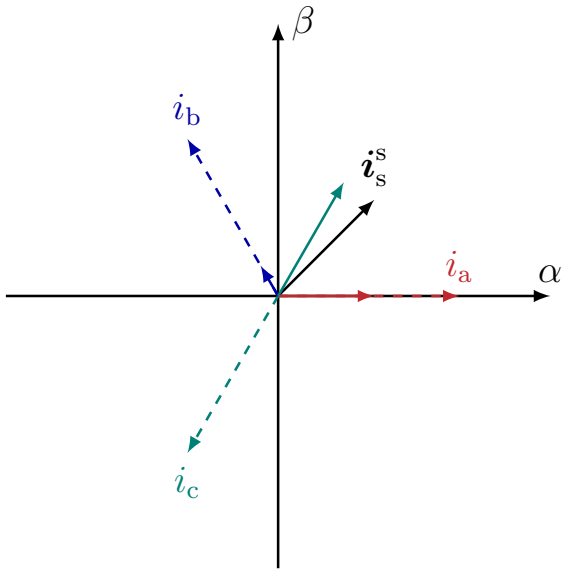

Figure 5: Phase voltages to space vector.

where ω_a is the reference frame angular speed. If synchronous reference speed is selected, the steady-state stator current is a constant value instead of a sinusoidally changing value. A common convention is to drop out superscript s in synchronous coordinates.

The asynchronous induction motor has two main components: stator and rotor. The stator is made out of three-phase windings that are distributed sinusoidally. Generally, the rotor is caged with aluminum or copper bars [18]. The stator current produces sinusoidally distributed flux that induces a current in the rotor bars. In addition, the rotor bars are affected by Lorenz force which produces electromechanical torque. The T-model in Figure 6 is a well-known induction motor model in the literature.

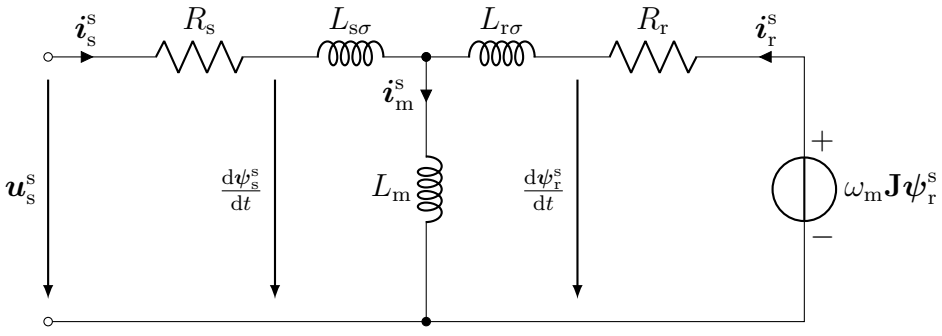

Figure 6: Dynamic T model.

The system is presented in stator coordinates, where the flux linkage equations

are

$$\boldsymbol{\psi}_\mathrm{s}^\mathrm{s} = L_{\mathrm{s}\sigma}\boldsymbol{i}_\mathrm{s}^\mathrm{s} + L_\mathrm{m}\boldsymbol{i}_\mathrm{m}^\mathrm{s} \tag{18a}$$
$$\boldsymbol{\psi}_\mathrm{r}^\mathrm{s} = L_{\mathrm{r}\sigma}\boldsymbol{i}_\mathrm{r}^\mathrm{s} + L_\mathrm{m}\boldsymbol{i}_\mathrm{m}^\mathrm{s} \tag{18b}$$

where $\boldsymbol{\psi}_\mathrm{s}^\mathrm{s}$ is stator flux linkage and $\boldsymbol{\psi}_\mathrm{r}^\mathrm{s}$ is rotor flux linkages, $L_{\mathrm{s}\sigma} = L_\mathrm{s} - L_\mathrm{m}$ is stator leakage inductance, $L_{\mathrm{r}\sigma} = L_\mathrm{r} - L_\mathrm{m}$ is rotor leakage inductance, and L_m is magnetizing inductance. The magnetizing current is a sum of stator and rotor currents $\boldsymbol{i}_\mathrm{m}^\mathrm{s} = \boldsymbol{i}_\mathrm{s}^\mathrm{s} + \boldsymbol{i}_\mathrm{r}^\mathrm{s}$. The voltage equations are expressed as

$$\frac{\mathrm{d}\boldsymbol{\psi}_\mathrm{s}^\mathrm{s}}{\mathrm{d}t} = \boldsymbol{u}_\mathrm{s}^\mathrm{s} - R_\mathrm{s}\boldsymbol{i}_\mathrm{s}^\mathrm{s} \tag{19a}$$
$$\frac{\mathrm{d}\boldsymbol{\psi}_\mathrm{r}^\mathrm{s}}{\mathrm{d}t} = \omega_\mathrm{m}\mathbf{J}\boldsymbol{\psi}_\mathrm{r}^\mathrm{s} - R_\mathrm{r}\boldsymbol{i}_\mathrm{r}^\mathrm{s} \tag{19b}$$

where $\boldsymbol{u}_\mathrm{s}^\mathrm{s}$ is stator voltage, R_s is stator resistance, R_r rotor resistance and $\mathbf{J} = \left[\begin{smallmatrix} 0 & -1 \\ 1 & 0 \end{smallmatrix}\right]$ is the orthogonal rotation matrix. However, the T-model is over-parametrized with five motor parameters, while only four parameters would sufficient without losing information.

The inverse-Γ model is based on T-model, but since actual rotor parameters are not needed, the turns ratio between the stator and rotor can be chosen arbitrarily. In the inverse-Γ model, the turns ratio is chosen in the manner that L_r and L_m are equal [19]. From this, the scaling factor is chosen as

$$\gamma = \frac{L_\mathrm{m}}{L_\mathrm{r}} = \frac{L_\mathrm{m}}{L_{\mathrm{r}\sigma} + L_\mathrm{m}}. \tag{20}$$

The scaled values in the inverse-Γ model are

$$L_\mathrm{M} = \gamma L_\mathrm{m} \tag{21a}$$
$$L_\sigma = \gamma L_{\mathrm{r}\sigma} + L_{\mathrm{s}\sigma} \tag{21b}$$
$$R_\mathrm{R} = \gamma^2 R_\mathrm{r}. \tag{21c}$$

The motor model with scaled values is shown in Figure 7. The corresponding flux equations are

$$\boldsymbol{\psi}_\mathrm{s}^\mathrm{s} = L_\sigma\boldsymbol{i}_\mathrm{s}^\mathrm{s} + \boldsymbol{\psi}_\mathrm{R}^\mathrm{s} \tag{22a}$$
$$\boldsymbol{\psi}_\mathrm{R}^\mathrm{s} = L_\mathrm{M}(\boldsymbol{i}_\mathrm{s}^\mathrm{s} + \boldsymbol{i}_\mathrm{R}^\mathrm{s}). \tag{22b}$$

The voltage equations are

$$\frac{\mathrm{d}\boldsymbol{\psi}_\mathrm{s}^\mathrm{s}}{\mathrm{d}t} = \boldsymbol{u}_\mathrm{s}^\mathrm{s} - R_\mathrm{s}\boldsymbol{i}_\mathrm{s}^\mathrm{s} \tag{23a}$$
$$\frac{\mathrm{d}\boldsymbol{\psi}_\mathrm{R}^\mathrm{s}}{\mathrm{d}t} = \omega_\mathrm{m}\mathbf{J}\boldsymbol{\psi}_\mathrm{R}^\mathrm{s} - R_\mathrm{R}\boldsymbol{i}_\mathrm{R}^\mathrm{s}. \tag{23b}$$

These equations can be transformed to synchronously rotating coordinates by

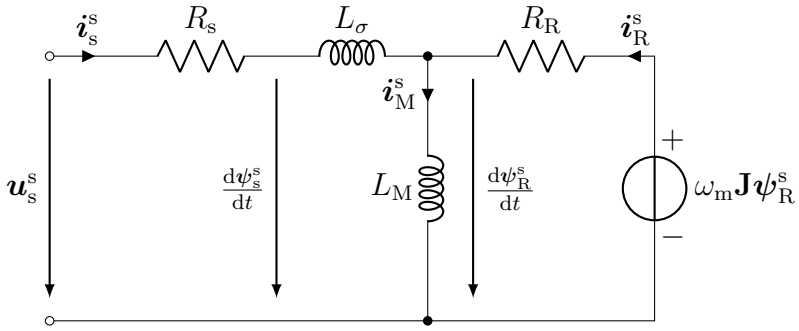

Figure 7: Dynamic inverse-Γ model.

choosing ω_s as the reference frame angular speed, resulting in equations

$$\frac{\mathrm{d}\boldsymbol{\psi}_\mathrm{s}}{\mathrm{d}t} = -R_\mathrm{s}\boldsymbol{i}_\mathrm{s} - \omega_\mathrm{s}\mathbf{J}\boldsymbol{\psi}_\mathrm{s} + \boldsymbol{u}_\mathrm{s} \tag{24a}$$

$$\frac{\mathrm{d}\boldsymbol{\psi}_\mathrm{R}}{\mathrm{d}t} = -R_\mathrm{R}\boldsymbol{i}_\mathrm{R} - \omega_\mathrm{r}\mathbf{J}\boldsymbol{\psi}_\mathrm{R}. \tag{24b}$$

Furthermore, flux linkage equations are transformed into synchronous coordinates

$$\boldsymbol{\psi}_\mathrm{s} = L_\sigma\boldsymbol{i}_\mathrm{s} + \boldsymbol{\psi}_\mathrm{R} \tag{25a}$$

$$\boldsymbol{\psi}_\mathrm{R} = L_\mathrm{M}(\boldsymbol{i}_\mathrm{s} + \boldsymbol{i}_\mathrm{R}) \tag{25b}$$

where the only change is the missing superscript s.

The stator current $\boldsymbol{i}_\mathrm{s}$ and the rotor flux $\boldsymbol{\psi}_\mathrm{R}$ are chosen as system state variables. These state variables are obtained by substituting equation (25a) to (24a) and equation (25b) to (24b), resulting in following state equations

$$L_\sigma\frac{\mathrm{d}\boldsymbol{i}_\mathrm{s}}{\mathrm{d}t} = -(R_\sigma\mathbf{I} + \omega_\mathrm{s}L_\sigma\mathbf{J})\boldsymbol{i}_\mathrm{s} + (\alpha\mathbf{I} - \omega_\mathrm{m}\mathbf{J})\boldsymbol{\psi}_\mathrm{R} + \boldsymbol{u}_\mathrm{s} \tag{26a}$$

$$\frac{\mathrm{d}\boldsymbol{\psi}_\mathrm{R}}{\mathrm{d}t} = R_\mathrm{R}\boldsymbol{i}_\mathrm{s} - (\alpha\mathbf{I} + \omega_\mathrm{r}\mathbf{J})\boldsymbol{\psi}_\mathrm{R} \tag{26b}$$

where $\alpha = R_\mathrm{R}/L_\mathrm{M}$ is the inverse rotor time constant, $R_\sigma = R_\mathrm{s} + R_\mathrm{R}$ is the total resistance, and $\mathbf{I} = \left[\begin{smallmatrix}1 & 0\\ 0 & 1\end{smallmatrix}\right]$ is the identity matrix. The electromagnetic torque is

$$\tau_\mathrm{m} = \frac{3p}{2}\boldsymbol{i}_\mathrm{s}^\mathrm{T}\mathbf{J}\boldsymbol{\psi}_\mathrm{R}. \tag{27}$$

A rigid mechanical subsystem for the motor is

$$I_\mathrm{M}\frac{\mathrm{d}\omega_\mathrm{m}}{\mathrm{d}t} = \tau_\mathrm{m} - \tau_\mathrm{L} \tag{28}$$

where τ_L is load torque.

Steady-state quantities are calculated by substituting $\frac{\mathrm{d}}{\mathrm{d}t} = 0$. The steady-state current is calculated from equation (26b) as

$$\boldsymbol{i}_\mathrm{s0} = \frac{\alpha\mathbf{I} + \omega_\mathrm{r0}\mathbf{J}}{R_\mathrm{R}}\boldsymbol{\psi}_\mathrm{R0} \tag{29}$$

where subscript 0 marks the steady-state operating point quantity. By applying the stator flux equation (25a) to (29) the steady-state rotor flux is obtained as

$$\boldsymbol{\psi}_{\mathrm{R0}} = \frac{R_{\mathrm{R}}}{L_\sigma}(\omega_{\mathrm{rb}}\mathbf{I} + \omega_{\mathrm{r0}}\mathbf{J})^{-1}\boldsymbol{\psi}_{\mathrm{s0}} \tag{30}$$

where $\omega_{\mathrm{rb}} = R_{\mathrm{R}}(1/L_{\mathrm{M}}+1/L_\sigma)$ is the breakdown slip frequency and $\boldsymbol{\psi}_{\mathrm{s0}}$ is steady-state stator flux linkage.

The steady-state torque is derived by substituting steady-state stator current (29) and the rotor flux (30) to electromagnetic torque equation (27), the steady-state torque is presented as

$$\tau_{\mathrm{m0}} = \frac{\psi_{\mathrm{R0}}^2\omega_{\mathrm{r0}}}{R_{\mathrm{R}}} = \frac{2\tau_{\mathrm{b0}}}{\omega_{\mathrm{r0}}/\omega_{\mathrm{rb}} + \omega_{\mathrm{rb}}/\omega_{\mathrm{r0}}} \tag{31a}$$

$$\tau_{\mathrm{b0}} = \frac{3p}{2}\frac{L_{\mathrm{M}}}{L_{\mathrm{M}}+L_\sigma}\frac{\psi_{\mathrm{s0}}^2}{2L_\sigma} \tag{31b}$$

where τ_{b0} is the breakdown torque. From (31a), the steady-state slip is derived as

$$\omega_{\mathrm{r0}} = \frac{\tau_{\mathrm{b0}}}{\tau_{\mathrm{m0}}}\left(1 - \sqrt{1 - \frac{\tau_{\mathrm{m0}}^2}{\tau_{\mathrm{b0}}^2}}\right)\omega_{\mathrm{rb}}. \tag{32}$$

3.2 V/Hz control

There are many different variants of V/Hz control. The simplest one is open-loop V/Hz control with constant stator flux reference. It is because the controller only increases voltage linearly with the frequency reference, keeping the stator flux approximately constant. The controller could include compensation for the voltage drop over the stator resistance (RI compensation). In the open-loop V/Hz control case the RI compensation could be implemented as a curve that boosts the voltage at low speeds. A proper RI compensation is crucial for constant flux at high loads and low speeds. The control law for open-loop control is

$$\boldsymbol{u}_{\mathrm{s,ref}} = \omega_{\mathrm{s}}\mathbf{J}\boldsymbol{\psi}_{\mathrm{s,ref}} \tag{33}$$

where $\boldsymbol{\psi}_{\mathrm{s,ref}}$ is the constant stator flux reference value. Even with perfect RI compensation, there are regions where the system could be unstable with open-loop control [8, 9].

The stability could be improved by adding feedback from stator currents through a compensator in Figure 8. The compensator includes RI compensation and a damping component from the stator current as

$$\boldsymbol{C}(s) = \frac{\alpha_{\mathrm{f}}}{s+\alpha_{\mathrm{f}}}R_{\mathrm{s}}\mathbf{I} - \frac{s}{s+\alpha_{\mathrm{f}}}\boldsymbol{K} \tag{34}$$

where α_{f} filter bandwidth and $\boldsymbol{K}$ is 2×2 gain matrix. Another feedback from the stator current is added to the stator angular frequency ω_{s}, where $F(s)$ is a high-pass filter and $\boldsymbol{k}^{\mathrm{T}}$ is 1×2 gain vector.

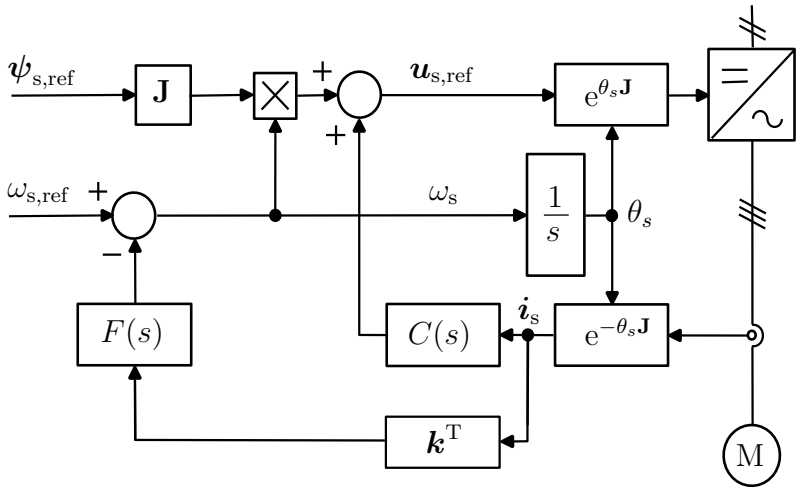

Figure 8: Compensated V/Hz control.

Including feedback from the stator current to the control law (33), the control law becomes

$$\boldsymbol{u}_{\mathrm{s,ref}} = \omega_{\mathrm{s}} \mathbf{J} \boldsymbol{\psi}_{\mathrm{s,ref}} + R_{\mathrm{s}} \boldsymbol{i}_{\mathrm{sf}} + \boldsymbol{K}(\boldsymbol{i}_{\mathrm{sf}} - \boldsymbol{i}_{\mathrm{s}}) \tag{35a}$$

$$\omega_{\mathrm{s}} = \omega_{\mathrm{s,ref}} + \boldsymbol{k}^{\mathrm{T}}(\boldsymbol{i}_{\mathrm{sf}} - \boldsymbol{i}_{\mathrm{s}}) \tag{35b}$$

where $\boldsymbol{i}_{\mathrm{sf}}$ is low-pass filtered current. The low-pass filtered current represents the operating point current, and it is calculated as

$$\frac{\mathrm{d}\boldsymbol{i}_{\mathrm{sf}}}{\mathrm{d}t} = \alpha_{\mathrm{f}}(\boldsymbol{i}_{\mathrm{s}} - \boldsymbol{i}_{\mathrm{sf}}). \tag{36}$$

The $\boldsymbol{K}$ and $\boldsymbol{k}$ gain matrices are calculated as [9]

$$\boldsymbol{K} = -R_{\mathrm{s}}\mathbf{I} + k_{\mathrm{u}} L_\sigma(\alpha \mathbf{I} + \omega_{\mathrm{m,ref}} \mathbf{J}) \tag{37a}$$

$$\boldsymbol{k} = \frac{k_\omega R_{\mathrm{R}} \mathbf{J} \boldsymbol{\psi}_{\mathrm{Rf}}}{\psi_{\mathrm{Rf}}^2} \tag{37b}$$

where k_{u} and k_ω are positive design parameters, $\psi_{\mathrm{Rf}} = \|\boldsymbol{\psi}_{\mathrm{Rf}}\|$ is the rotor-flux magnitude, and the operating point for rotor flux is estimated from stator flux reference and low-pass filtered stator current $\boldsymbol{\psi}_{\mathrm{Rf}} = \boldsymbol{\psi}_{\mathrm{s,ref}} - L_\sigma \boldsymbol{i}_{\mathrm{sf}}$ [9].

3.2.1 Observer-based V/Hz control

The observer-based V/Hz control is something between sensorless field-oriented control and conventional V/Hz control. It utilizes a flux observer and state-feedback control law as shown in Figure 9. The observer is a reduced-order flux observer.

The state-feedback control law is

$$\boldsymbol{u}_{\mathrm{s,ref}} = R_{\mathrm{s}} \boldsymbol{i}_{\mathrm{s}} + \omega_{\mathrm{s}} \mathbf{J} \boldsymbol{\psi}_{\mathrm{s,ref}} + \boldsymbol{K}_{\mathrm{s}}(\boldsymbol{\psi}_{\mathrm{s,ref}} - \hat{\boldsymbol{\psi}}_{\mathrm{s}}) \tag{38}$$

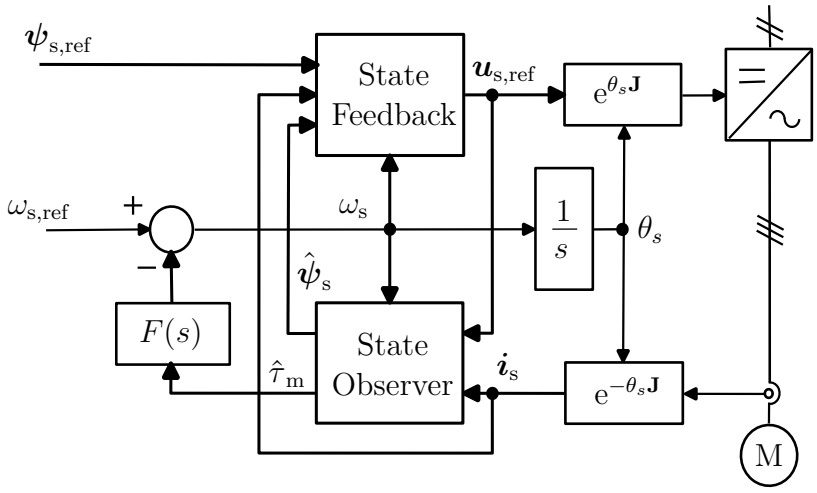

Figure 9: Observer-based V/Hz control.

where $\boldsymbol{K}_{\mathrm{s}}$ is 2×2 gain matrix and $\hat{\boldsymbol{\psi}}_{\mathrm{s}}$ is stator flux estimate provided by state-observer. The state-feedback control law could be rewritten since the reduced-order flux observer is used $\hat{\boldsymbol{\psi}}_{\mathrm{s}} = \hat{\boldsymbol{\psi}}_{\mathrm{R}} + L_\sigma \boldsymbol{i}_{\mathrm{s}}$ holds. The modified state-feedback is

$$\boldsymbol{u}_{\mathrm{s,ref}} = R_{\mathrm{s}} \boldsymbol{i}_{\mathrm{s}} + \omega_{\mathrm{s}} \mathbf{J} \boldsymbol{\psi}_{\mathrm{s,ref}} + \boldsymbol{K}_{\mathrm{s}} (\boldsymbol{i}_{\mathrm{s,ref}} - \boldsymbol{i}_{\mathrm{s}}) \tag{39a}$$

$$\boldsymbol{i}_{\mathrm{s,ref}} = \frac{\boldsymbol{\psi}_{\mathrm{s,ref}} - \hat{\boldsymbol{\psi}}_{\mathrm{R}}}{L_\sigma} \tag{39b}$$

where $\boldsymbol{i}_{\mathrm{s,ref}}$ is an intermediate stator current reference, that could be saturated to limit maximum current. The stator angular frequency is expressed as

$$\omega_{\mathrm{s}} = \omega_{\mathrm{s,ref}} - k_\omega (\hat{\tau}_{\mathrm{m}} - \hat{\tau}_{\mathrm{mf}}) \tag{40}$$

where k_ω is a positive design parameter for damping, $\hat{\tau}_{\mathrm{m}}$ is estimated torque, and $\hat{\tau}_{\mathrm{mf}}$ is low-pass filtered torque estimate. The stator frequency could be expressed as

$$\omega_{\mathrm{s}} = \omega_{\mathrm{s,ref}} - \underbrace{\frac{k_\omega s}{s + \alpha_{\mathrm{f}}}}_{F(s)} \hat{\tau}_{\mathrm{m}} \tag{41}$$

where $F(s)$ is a high-pass filter. [10]

The reduced-order flux observer is based on (26b) and is expressed as

$$\frac{\mathrm{d}\hat{\boldsymbol{\psi}}_{\mathrm{R}}}{\mathrm{d}t} = \boldsymbol{u}_{\mathrm{s,ref}} - (R_{\mathrm{s}} \mathbf{I} + \omega_{\mathrm{s}} L_\sigma \mathbf{J}) \boldsymbol{i}_{\mathrm{s}} - L_\sigma \frac{\mathrm{d}\boldsymbol{i}_{\mathrm{s}}}{\mathrm{d}t} - \omega_{\mathrm{s}} \mathbf{J} \hat{\boldsymbol{\psi}}_{\mathrm{R}} + \boldsymbol{K}_{\mathrm{o}} \boldsymbol{e} \tag{42}$$

where $\boldsymbol{K}_{\mathrm{o}}$ is 2×2 gain matrix for the observer and $\boldsymbol{e}$ is correction vector, which is obtained from (26a) as

$$\boldsymbol{e} = L_\sigma \frac{\mathrm{d}\boldsymbol{i}_{\mathrm{s}}}{\mathrm{d}t} + (R_\sigma \mathbf{I} + \omega_{\mathrm{s}} L_\sigma \mathbf{J}) \boldsymbol{i}_{\mathrm{s}} - (\alpha \mathbf{I} - \hat{\omega}_{\mathrm{m}} \mathbf{J}) \hat{\boldsymbol{\psi}}_{\mathrm{R}} - \boldsymbol{u}_{\mathrm{s,ref}}. \tag{43}$$

The outputs from the observer are

$$\hat{\boldsymbol{\psi}}_\mathrm{s} = \hat{\boldsymbol{\psi}}_\mathrm{R} + L_\sigma \boldsymbol{i}_\mathrm{s} \tag{44a}$$

$$\hat{\tau}_\mathrm{m} = \boldsymbol{i}_\mathrm{s}^\mathrm{T} \mathbf{J} \hat{\boldsymbol{\psi}}_\mathrm{R}. \tag{44b}$$

The motor speed is estimated as

$$\frac{\mathrm{d}\hat{\omega}_\mathrm{m}}{\mathrm{d}t} = \alpha_\mathrm{o} \frac{\hat{\boldsymbol{\psi}}_\mathrm{R}^\mathrm{T} \mathbf{J} \boldsymbol{e}}{\|\hat{\boldsymbol{\psi}}_\mathrm{R}\|^2} \tag{45}$$

where α_o is speed estimation bandwidth. [10]

The observer can be called inherently sensorless if gain fulfills $\boldsymbol{K}_\mathrm{o} \mathbf{J} \hat{\boldsymbol{\psi}}_\mathrm{R} = 0$, then the speed-dependent term disappears from (43). The observer gain used is

$$\boldsymbol{K}_\mathrm{o} = \frac{2\sigma_\mathrm{o}(\alpha \mathbf{I} + \hat{\omega}_\mathrm{m} \mathbf{J})}{\alpha^2 + \hat{\omega}_\mathrm{m}^2} \frac{\hat{\boldsymbol{\psi}}_\mathrm{R} \hat{\boldsymbol{\psi}}_\mathrm{R}^\mathrm{T}}{\|\hat{\boldsymbol{\psi}}_\mathrm{R}\|^2} \tag{46}$$

where σ_o is the exponential decay rate of estimation error. The decay rate is chosen as

$$\sigma_\mathrm{o} = \zeta_\infty |\omega_\mathrm{s}| + \alpha/2. \tag{47}$$

The state-feedback gain matrix is

$$\boldsymbol{K}_\mathrm{s} = \sigma_\mathrm{c} \mathbf{I} \tag{48}$$

where σ_c approximately corresponds to closed-loop bandwidth. [10]

3.3 Linearized models

The induction motor is a nonlinear system. The system is linearized at the steady-state operating to use linear system analysis. When the system is linearized the local stability of the operating point could be analyzed using the transfer function. First, the small-signal motor model is derived. Then motor control methods are included in the motor model.

3.3.1 Motor model

The linearization is accomplished with the Taylor series expansion. These linearized quantities are marked with Δ, e.g., the linearized stator current is $\Delta \boldsymbol{i}_\mathrm{s} = \boldsymbol{i}_\mathrm{s} - \boldsymbol{i}_\mathrm{s0}$. Linearising stator current dynamics (26a) results

$$\begin{aligned} \frac{\mathrm{d}\Delta \boldsymbol{i}_\mathrm{s}}{\mathrm{d}t} = &- \left(\frac{R_\sigma}{L_\sigma} \mathbf{I} + \omega_\mathrm{s0} \mathbf{J} \right) \Delta \boldsymbol{i}_\mathrm{s} + \frac{1}{L_\sigma} (\alpha \mathbf{I} - \omega_\mathrm{m0} \mathbf{J}) \Delta \boldsymbol{\psi}_\mathrm{R} + \frac{1}{L_\sigma} \Delta \boldsymbol{u}_\mathrm{s} \\ &- \mathbf{J} \boldsymbol{i}_\mathrm{s0} \Delta \omega_\mathrm{s} - \frac{1}{L_\sigma} \mathbf{J} \boldsymbol{\psi}_\mathrm{R0} \Delta \omega_\mathrm{m} \end{aligned} \tag{49}$$

where terms $\Delta\omega_\mathrm{s}$ and $\Delta\omega_\mathrm{m}$ are new linearized input terms for the systems. Linearising rotor flux dynamics (26b) results

$$\frac{\mathrm{d}\Delta\boldsymbol{\psi}_\mathrm{R}}{\mathrm{d}t} = R_\mathrm{R}\Delta\boldsymbol{i}_\mathrm{s} - (\alpha\mathbf{I} + \omega_\mathrm{r0}\mathbf{J})\Delta\boldsymbol{\psi}_\mathrm{R} - \mathbf{J}\boldsymbol{\psi}_\mathrm{R0}\Delta\omega_\mathrm{s} + \mathbf{J}\boldsymbol{\psi}_\mathrm{R0}\Delta\omega_\mathrm{m} \tag{50}$$

and linearized torque is

$$\Delta\tau_\mathrm{m} = -\boldsymbol{\psi}_\mathrm{R0}\mathbf{J}\Delta\boldsymbol{i}_\mathrm{s} + \boldsymbol{i}_\mathrm{s0}\mathbf{J}\Delta\boldsymbol{\psi}_\mathrm{R}. \tag{51}$$

The Linearized torque is formed from two terms, which originate from the stator current and rotor flux deviations. From equations (49) and (50), state-space matrices are acquired as [9]

$$\begin{aligned}\frac{\mathrm{d}\Delta\boldsymbol{x}}{\mathrm{d}t} = &\underbrace{\begin{bmatrix} -\frac{R_\sigma}{L_\sigma}\mathbf{I} - \omega_\mathrm{s0}\mathbf{J} & \frac{1}{L_\sigma}(\alpha\mathbf{I} - \omega_\mathrm{m0}\mathbf{J}) \\ R_\mathrm{R}\mathbf{I} & -(\alpha\mathbf{I} + \omega_\mathrm{r0}\mathbf{J}) \end{bmatrix}}_{\boldsymbol{A}}\Delta\boldsymbol{x} \\ &+ \underbrace{\begin{bmatrix} -\frac{1}{L_\sigma}\mathbf{I} \\ \mathbf{0} \end{bmatrix}}_{\boldsymbol{B}_\mathrm{s}}\Delta\boldsymbol{u}_\mathrm{s} - \underbrace{\begin{bmatrix} \mathbf{J}\boldsymbol{i}_\mathrm{s0} \\ \mathbf{J}\boldsymbol{\psi}_\mathrm{R0} \end{bmatrix}}_{\boldsymbol{b}_\mathrm{s}}\Delta\omega_\mathrm{s} + \underbrace{\begin{bmatrix} -\frac{1}{L_\sigma}\mathbf{J}\boldsymbol{\psi}_\mathrm{R0} \\ \mathbf{J}\boldsymbol{\psi}_\mathrm{R0} \end{bmatrix}}_{\boldsymbol{b}_\mathrm{m}}\Delta\omega_\mathrm{m}\end{aligned} \tag{52a}$$

where $\Delta\boldsymbol{x} = [\Delta\boldsymbol{i}_\mathrm{s}^\mathrm{T}, \Delta\boldsymbol{\psi}_\mathrm{R}^\mathrm{T}]^\mathrm{T}$ is 4×1 state vector and $\mathbf{0} = \left[\begin{smallmatrix} 0 & 0 \\ 0 & 0 \end{smallmatrix}\right]$ is the zero matrix. Linearized output matrices are presented as

$$\Delta\boldsymbol{i}_\mathrm{s} = \underbrace{\begin{bmatrix} \mathbf{I} & \mathbf{0} \end{bmatrix}}_{\boldsymbol{C}_\mathrm{s}}\Delta\boldsymbol{x} \tag{52b}$$

$$\Delta\boldsymbol{\psi}_\mathrm{s} = \underbrace{\begin{bmatrix} L_\sigma\mathbf{I} & \mathbf{I} \end{bmatrix}}_{\boldsymbol{C}}\Delta\boldsymbol{x} \tag{52c}$$

$$\Delta\tau_\mathrm{m} = \underbrace{\begin{bmatrix} -\boldsymbol{\psi}_\mathrm{R0}^\mathrm{T}\mathbf{J} & -\boldsymbol{i}_\mathrm{s0}^\mathrm{T}\mathbf{J} \end{bmatrix}}_{\boldsymbol{c}_\mathrm{m}}\Delta\boldsymbol{x}. \tag{52d}$$

3.3.2 V/Hz control

When linearizing V/Hz control, simplification is made to reduce the system order. The low-pass filtered current $\boldsymbol{i}_\mathrm{sf} = \boldsymbol{i}_\mathrm{s0}$ is assumed to be a steady-state current when the filter bandwidth is selected low enough. The assumption holds, but then the low-pass filter dynamics (36) is omitted.

Linearizing the control law results

$$\Delta\boldsymbol{u}_\mathrm{s,ref} = -(\boldsymbol{K} + \mathbf{J}\boldsymbol{\psi}_\mathrm{s,ref}\boldsymbol{k}^\mathrm{T})\Delta\boldsymbol{i}_\mathrm{s}, \quad \Delta\omega_\mathrm{s} = -\boldsymbol{k}^\mathrm{T}\Delta\boldsymbol{i}_\mathrm{s}. \tag{53}$$

By substituting (53) into (52a) with the ouput (52b), the closed-loop system matrix is obtained as

$$\boldsymbol{A}_\mathrm{cc} = \boldsymbol{A} - [\boldsymbol{B}_\mathrm{s}(\boldsymbol{K} + \mathbf{J}\boldsymbol{\psi}_\mathrm{s0}\boldsymbol{k}^\mathrm{T}) + \boldsymbol{b}_\mathrm{s}\boldsymbol{k}^\mathrm{T}]\boldsymbol{C}_\mathrm{s}. \tag{54}$$

The transfer function from motor speed to electromagnetic torque is derived as

$$G_{\mathrm{C}}(s) = -\frac{\Delta\tau_{\mathrm{m}}(s)}{\Delta\omega_{\mathrm{m}}(s)} = -\boldsymbol{c}_{\mathrm{m}}(s\mathbf{I}_4 - \boldsymbol{A}_{\mathrm{cc}})^{-1}\boldsymbol{b}_{\mathrm{m}} \tag{55}$$

where $\mathbf{I}_4$ is the 4×4 identity matrix [9]. Equation (55) could be used to analyze both fully open-loop V/Hz control and V/Hz control with the compensator. To analyze the open-loop V/Hz controller, the feedback gains k_{u} and k_ω are set to zero. Furthermore, when the open-loop control is analyzed, the simplifications do not affect the analytical solution, and the result is accurate.

3.3.3 Observer-based V/Hz control

Linearizing the observer-based control starts with linearization of the control law (38) as

$$\Delta\boldsymbol{u}_{\mathrm{s}} = -\boldsymbol{K}_{\mathrm{c}}\Delta\boldsymbol{x} + \boldsymbol{K}_{\mathrm{s}}\Delta\tilde{\boldsymbol{\psi}}_{\mathrm{R}} + \boldsymbol{N}\Delta\boldsymbol{\psi}_{\mathrm{s,ref}} + \mathbf{J}\boldsymbol{\psi}_{\mathrm{s0}}\Delta\omega_{\mathrm{s}} \tag{56}$$

where $\Delta\tilde{\boldsymbol{\psi}}_{\mathrm{R}} = \boldsymbol{\psi}_{\mathrm{R}} - \Delta\hat{\boldsymbol{\psi}}_{\mathrm{R}}$ is the rotor flux estimation error, $\boldsymbol{K}_{\mathrm{c}} = [L_\sigma\boldsymbol{K}_{\mathrm{s}} - R_{\mathrm{s}}\mathbf{I}, \boldsymbol{K}_{\mathrm{s}}]$ is the state-feedback gain matrix, and $\boldsymbol{N} = \omega_{\mathrm{s0}}\mathbf{J} + \boldsymbol{K}_{\mathrm{s}}$ is the reference-feedforward matrix. To get the closed-loop system, the linearized control law (56) is inserted into linearized motor model (52a) resulting

$$\frac{\mathrm{d}\Delta\boldsymbol{x}}{\mathrm{d}t} = \boldsymbol{A}_{\mathrm{co}}\Delta\boldsymbol{x} + \boldsymbol{B}_{\mathrm{s}}\boldsymbol{K}_{\mathrm{s}}\Delta\tilde{\boldsymbol{\psi}}_{\mathrm{R}} + \boldsymbol{B}_{\mathrm{s}}\boldsymbol{N}\Delta\boldsymbol{\psi}_{\mathrm{s,ref}} + \boldsymbol{b}_{\mathrm{m}}\Delta\omega_\delta \tag{57}$$

where $\boldsymbol{A}_{\mathrm{co}} = \boldsymbol{A} - \boldsymbol{B}_{\mathrm{s}}\boldsymbol{K}_{\mathrm{c}}$ is closed-loop system matrix. The transfer function is [10]

$$G_{\mathrm{o}}(s) = \frac{\Delta\tau_{\mathrm{m}}(s)}{\Delta\omega_\delta(s)} = \boldsymbol{c}_{\mathrm{m}}(s\mathbf{I}_4 - \boldsymbol{A}_{\mathrm{co}})^{-1}\boldsymbol{b}_{\mathrm{m}} = \frac{\psi_{\mathrm{R0}}^2}{R_{\mathrm{R}}}\frac{\omega_{\mathrm{rb}}s + \omega_{\mathrm{rb}}^2 - \omega_{\mathrm{r0}}^2}{(s+\omega_{\mathrm{rb}})^2 + \omega_{\mathrm{r0}}^2} \tag{58}$$

where $\psi_{\mathrm{R0}} = \|\boldsymbol{\psi}_{\mathrm{R0}}\|$ is the magnitude of steady-state rotor flux. The state-feedback control law (38) does not affect the stability. It can be shown that the transfer function (58) is strictly passive for the whole feasible operating region since $\mathrm{Re}\{G_o(s)\} > 0$ if $|\omega_{\mathrm{r0}}| < \omega_{\mathrm{rb}}$ and $\psi_{\mathrm{R0}} > 0$. This implies that the system is robust to unknown mechanics. As long as the mechanical system is passive, the system is stable. [10]

The damping could be increased via stator frequency high-pass filter (40) seen in Figure 10. Including the high-pass filter $F(s)$ in Figure 10 into the transfer function (58) results in

$$G_{\mathrm{co}}(s) = \frac{\omega_{\mathrm{rb}}s + \omega_{\mathrm{rb}}^2 - \omega_{\mathrm{r0}}^2}{[(s+\omega_{\mathrm{rb}})^2 + \omega_{\mathrm{r0}}^2]/\lambda + F(s)(\omega_{\mathrm{rb}}s + \omega_{\mathrm{rb}}^2 - \omega_{\mathrm{r0}}^2)} \tag{59}$$

where $\lambda = \psi_{\mathrm{R0}}^2/R_{\mathrm{R}}$.

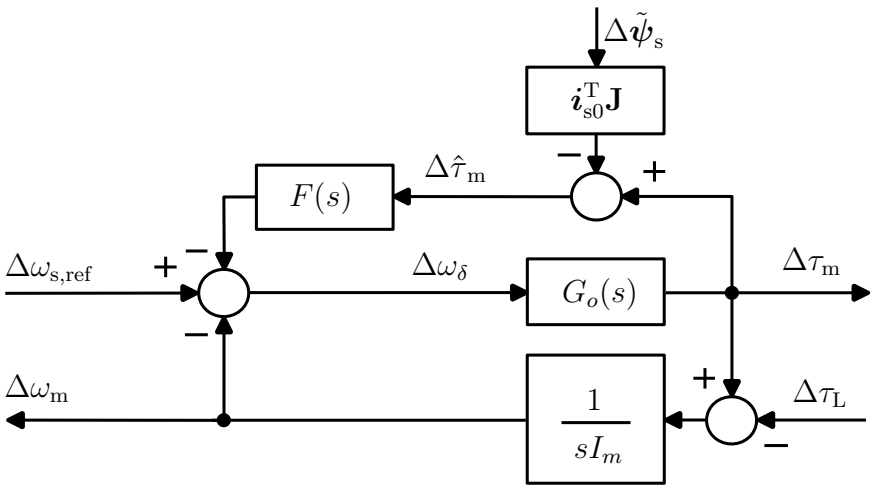

Figure 10: Linearized closed-loop system for observer-based V/Hz control.

4 Results

The results of this thesis are split into two sections. In section 4.1, the implementation for the identification of the frequency response is presented. The implementation is based on the method presented in section 2.3 with frequency by frequency injection. The algorithm is implemented in the *motulator* platform [20]. In section 4.2, the comparisons are carried out between analytical models and identified frequency responses from time-domain simulations.

4.1 Implementation

The method presented in section 2.3 could be implemented with any simulator that can model the motor, i.e., it could be implemented with Matlab, Python, or any other programming language. In this thesis method is implemented with the *motulator* motor drive simulator [20]. With this method, the controller could be a black box that has an interface for motor parameters, reference values, inputs for measurements, and output for the motor electrical subsystem.

The flow chart of the identification program is shown in Figure 11. Inputs for the program are motor, controller type, operating point, frequency response range, and resolution. If only the speed reference and the torque are known from the operating point, the motor is driven to that operating point. When the motor is in a steady-state, sinusoidal injection starts with the desired frequency. After the simulation is completed, phasor values for the excitation frequency are obtained from motor speed and torque with the discrete Fourier transformation. If all excitation frequencies are simulated, the data is saved as a mat file. If there are still sinusoids that are not simulated, the program loops back and selects the next frequency. If frequency response from several operating points, motors, or controllers is needed, an outer *for*-loop could be implemented to achieve this.

There are multiple ways to implement the signal injection into motor speed. One way to implement the signal injection in motor speed is to replace the mechanical subsystem (28). The solver used in the simulations requires the derivative of motor speed. To obtain the sinusoidally changing motor speed with constant amplitude, the sinewave must be derivate resulting function for the solver is

$$\frac{\mathrm{d}\omega_\mathrm{M}}{\mathrm{d}t} = \omega A \cos(\omega t) \tag{60}$$

where ω is the excitation signal angular frequency and A is the amplitude of the excitation signal.

When using the switching method between the mechanical subsystem and the excitation signal the benefit is the initial motor states do not need to be known and only the desired operating point is enough. The motor could be driven to the desired operating point with the mechanical subsystem. Then the mechanical subsystem (28) is replaced with the signal injection (60). The change is done with an *if* statement, at the sinusoidal injection step from the flow chart in Figure 11. The change between mechanical subsystem (28) and the signal injection (60) has to be done at specific

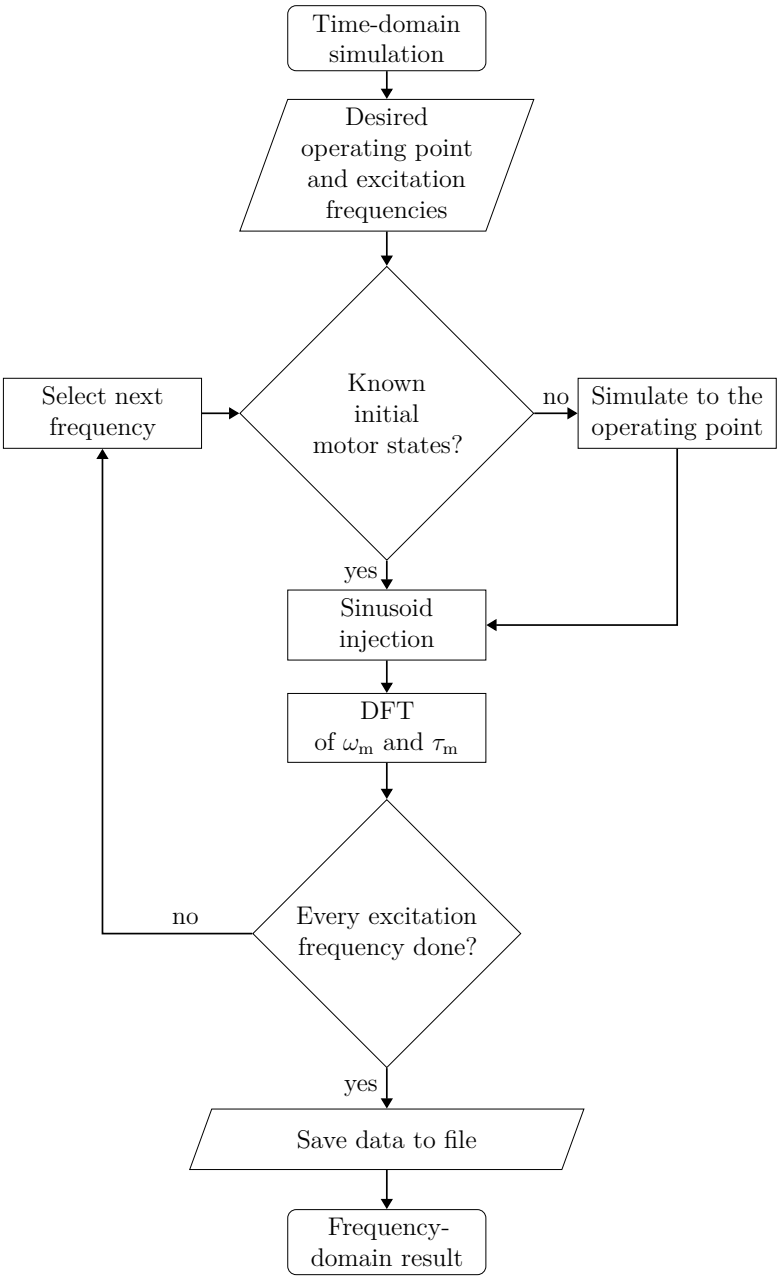

Figure 11: Flow chart of the program

times. Otherwise, the operating point will change shown in Figure 12. The switching instance is dependent on the excitation frequency ω. The correct time is where $\cos(\omega t) = \pm 1$ in (60). If the change is done at the point where $\cos(\omega t) = 0$ in (60) the motor speed ω_M will increase (Fig.12) and the electromagnetic torque will decrease. As a result the operating point shifts.

After the signal injection into motor speed is simulated with the desired frequency, the phasor for the angular frequency is obtained with DFT. Then the algorithm checks if there are other excitation frequencies still that need to be simulated. If

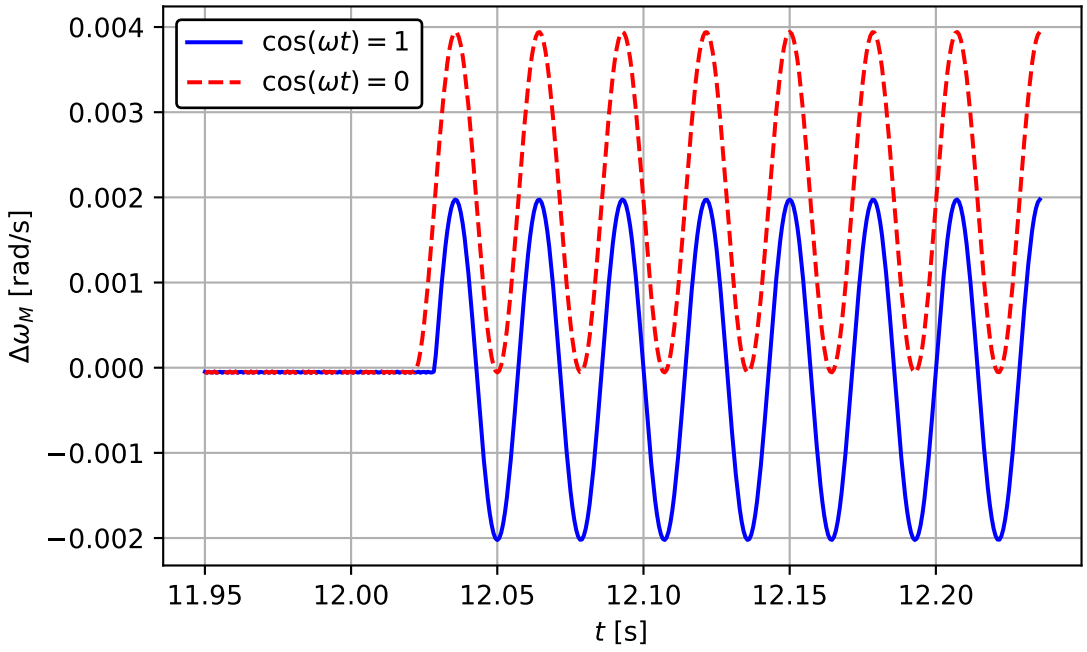

Figure 12: Shift in the operating point is caused by an incorrect switching time between the mechanical subsystem and the signal injection.

yes it continues until every frequency is done. Otherwise, the algorithm sorts the frequency responses and saves them as a mat file. After the data is obtained, the steady-state value has to be subtracted from the frequency response. Therefore, a simulation where amplitude $A = 0$ (60) has to be done, to obtain the steady-state effect.

Each frequency in the frequency response is one simulation. To reduce the simulation time an asynchronous multi-processing is used from Python library multiprocessing [21]. The program assigns a pool of workers where the number of workers depends on the number of cores in the central processing unit. Each worker takes one excitation frequency to simulate and returns the result after the simulation is done. The worker takes the next available excitation frequency.

4.2 Comparison

This section shows a comparison between identified frequency responses from time-domain simulations and analytical solutions (55) and (59). Parameters of a 45-kW induction motor were used shown in Table 1. The operating point is chosen to be at 80% of nominal speed ω_n and torque τ_n. In the time-domain simulations, pulse width modulation is omitted, the inverter is assumed to be lossless $\boldsymbol{u}_\mathrm{s} = \boldsymbol{u}_\mathrm{s,ref}$, and constant DC bus voltage is used.

The motor is controlled with three different control methods: open-loop V/Hz control, compensator-based V/Hz control, and observer-based V/Hz control. The

stator flux reference is chosen to be constant and nominal as

$$\boldsymbol{\psi}_{\mathrm{s,ref}} = [u_{\mathrm{n}}/(2\pi f_{\mathrm{n}}), 0]^{\mathrm{T}} \tag{61}$$

where u_{n} is the motor nominal phase voltage peak value and f_{n} is the motor nominal frequency obtained from the motor nominal frequency. There is no parameter error in the controller motor parameters. In simulations, the controller works in discrete time with sampling frequency $f_{\mathrm{s}} = 4$ kHz, while the motor is modeled in continuous time. The motor speed and electromagnetic torque are sampled at the rate of 80 kHz for the discrete Fourier transformation.

Table 1: Data of the 45 kW induction motor.

Nominal values	
u_{n}	$\sqrt{2/3}$ 400 V
i_{n}	$\sqrt{2}$ 81 A
f_{n}	50 Hz
N	1477 r/min
τ_{n}	291 Nm
Parameters	
R_{s}	60 mΩ
R_{R}	30 mΩ
L_{σ}	2.2 mH
L_{M}	24.5 mH
p	2

Analytical frequency responses are obtained from the transfer functions (55) and (59) by substituting the $s = \mathrm{j}\omega$. The identified frequency response has a resolution of 250 linearly spaced samples for frequencies from 0.1 Hz to 100 Hz.

4.2.1 Open-loop V/Hz control

First, the fully open-loop controlled system frequency responses from the rotor speed to the electromagnetic torque (55) are compared in Figure 13. In both analytical and identification cases, the controller gains k_{ω} and k_{u} are set to zero in equation (37) and RI compensation is omitted. Indeed, the identified frequency response matches the analytical solution. It should be noted that this control method closely resembles a direct online motor behavior. That is why the result has the same shape as in article [7].

The open-loop control has a nonpassive region just below the input frequency between 24.7 Hz to 39.5 Hz. In this region, the electromagnetic damping becomes negative since the angle goes under -90 degrees. Instead of dissipating the torsional vibration in the electromagnetic damping, it could increase it. Additionally, the system might not need any excitation if the torsional natural frequency is inside the

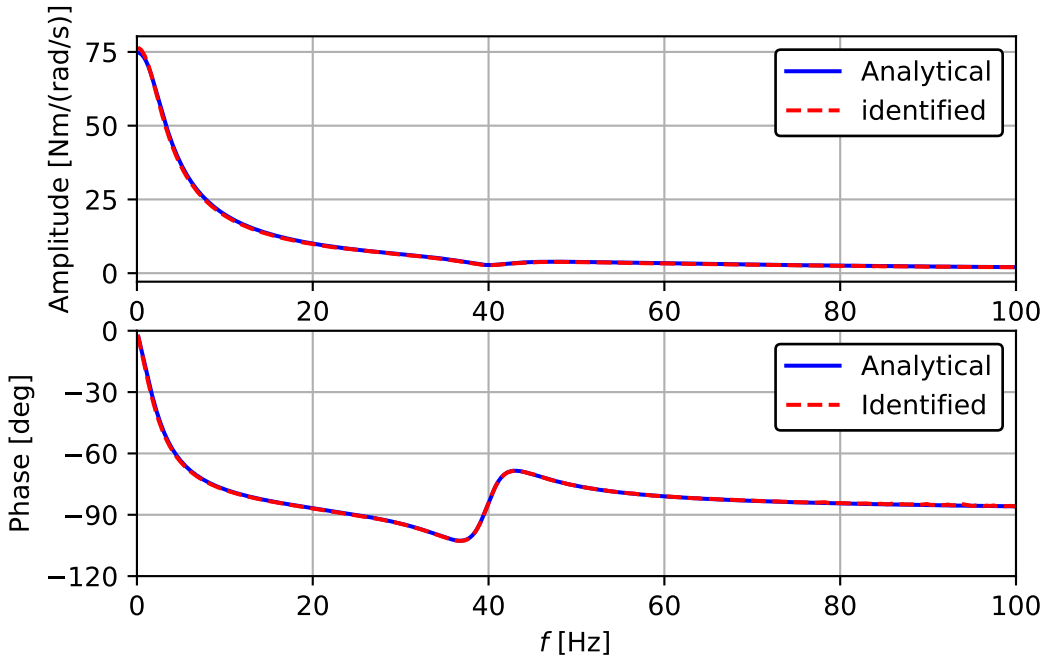

Figure 13: Frequency response from the rotor speed ω_{m} to the electromagnetic torque τ_{m} with open-loop V/Hz control.

nonpassive area, assuming that the mechanical system has lower damping than the negative damping from the electromagnetic system. This implies that the system could become unstable.

4.2.2 V/Hz control

The second comparison uses V/Hz control with compensator (34). The analytical solution for transfer function (55) is the same as in the open-loop control, but the controller gains k_ω and k_{u} are parametrized according to Table 2.

Table 2: Closed-loop V/Hz control parameters.

Positive design parameter	k_{u}	0.6	-
Positive design parameter	k_ω	4	-
Low-pass filter bandwidth	α_{f}	$0.1\omega_{\mathrm{rb}}$	rad/s

Comparing the analytical solution and identified result in Figure 14, it can be seen that the basic shape is nearly the same. Then again this can be expected since the low-pass filter dynamics (36) were omitted. Furthermore, by comparing open-loop control Figure 13 to conventional V/Hz control Figure 14, it can be seen that the nonpassive region between 24.7 - 39.5 Hz disappears. Implying that the

control and electrical system are passive at this operating point since there is no negative damping.

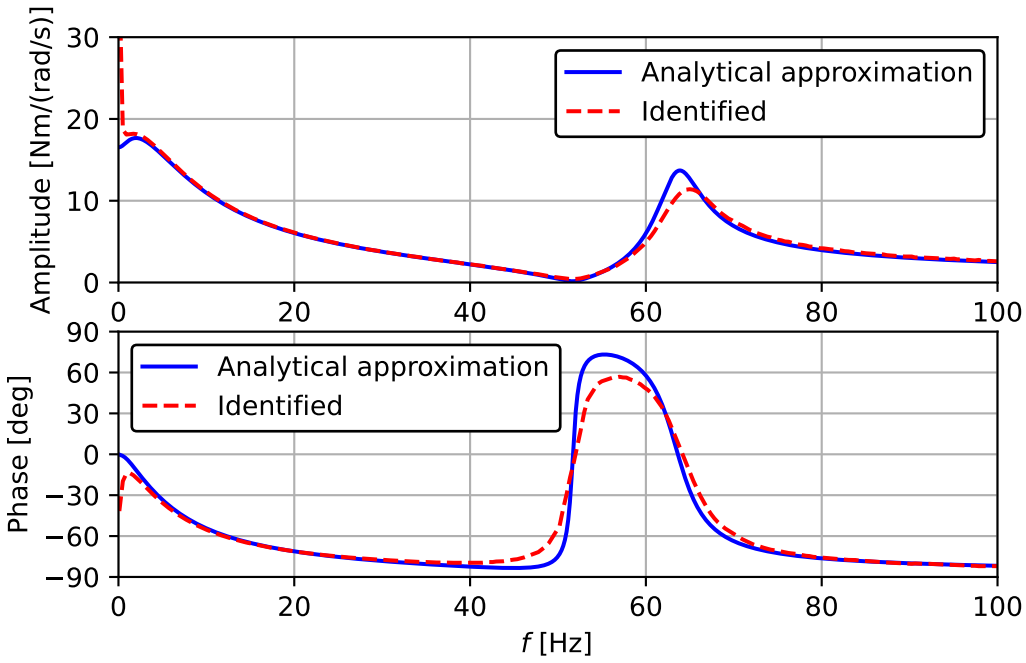

Figure 14: Frequency response from the rotor speed ω_{m} to the electromagnetic torque τ_{m} with V/Hz control.

4.2.3 Observer-based V/Hz control

Lastly, the identified frequency response of the observer-based V/Hz control is compared to the analytical solution (59). The only assumption in the analytical solution is the linearization [10]. The controller uses parameters given in Table 3.

Table 3: Observer based-V/Hz control parameters.

State-feedback gain	σ_{c}	$2\pi \cdot 20$	rad/s
High-pass filter bandwidth	α_{f}	$2\pi \cdot 1$	rad/s
Damping gain	k_ω	0.5	$(\mathrm{Nm} \cdot \mathrm{s})^{-1}$
Observer damping-ratio	ζ_∞	0.7	-
Speed-estiamtion bandwidth	α_{o}	$2\pi \cdot 40$	rad/s

The comparison is shown in Figure 15. It can be seen that the identified result starts to diverge from the analytical solution at the frequency of 20 Hz. This is caused

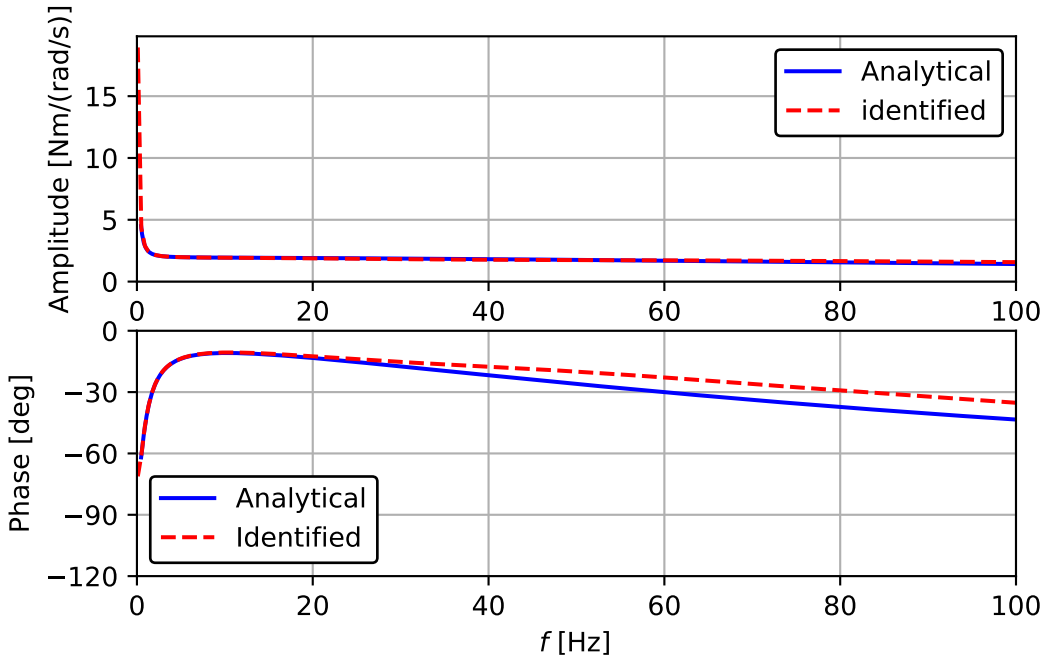

Figure 15: Frequency response from the rotor speed ω_{m} to the electromagnetic torque τ_{m} with observer-based V/Hz control and 4 kHz sampling frequency.

by digital time delays since the analytical solution is formulated in continuous time and the identified frequency response is simulated with a discrete-time controller.

The difference caused by digital time delays can be confirmed by increasing the sampling frequency of the controller. The sampling frequency is increased from 4 kHz to 40 kHz, this shifts the difference originating from the digital time delays to higher frequencies. Figure 16 shows that the sampling frequency plays a role in the difference.

Comparing the frequency response of the observer-based V/Hz control with the open-loop control, it can be seen that there is no nonpassive region between 24.7 Hz to 39.5 Hz. Moreover, if the mechanical system is passive, the whole system is passive and therefore stable. To summarize the results, it could be said that the frequency response can be obtained from the time-domain simulations. Also, the controller has a significant role in the passivity of the electromagnetic system seen by mechanics.

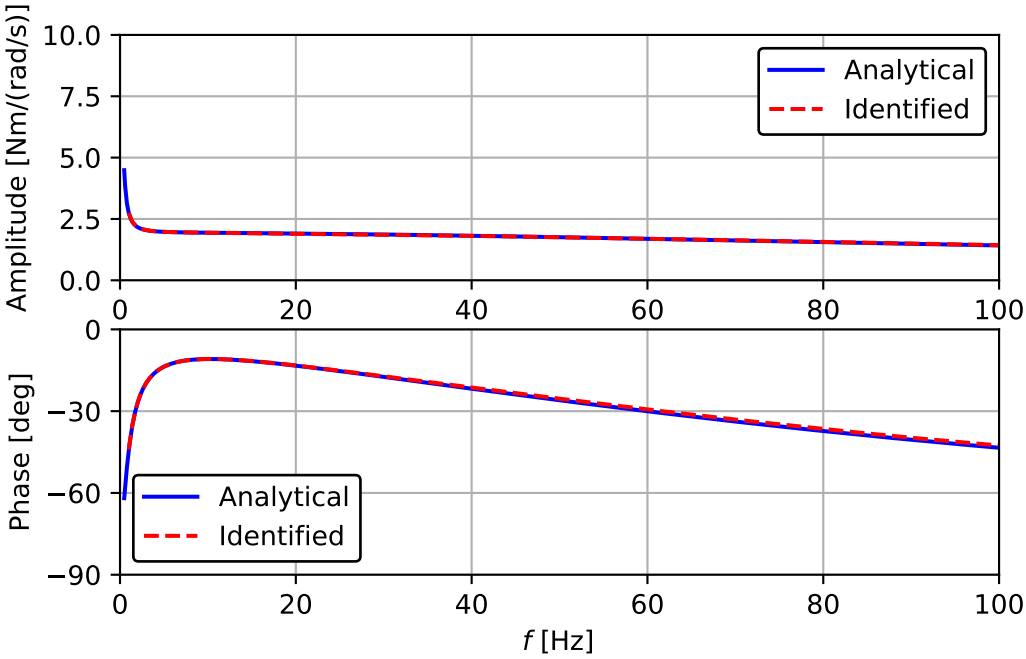

Figure 16: Frequency response from the rotor speed ω_{m} to the electromagnetic torque τ_{m} with observer-based V/Hz control and 40 kHz sampling frequency.

5 Conclusion

The goal of this thesis was to develop and validate a method to obtain controlled motor frequency response between motor speed and electromagnetic torque from time-domain simulations. The proposed method combines a well-known frequency-by-frequency identification method for linear time-invariant systems with a small-signal injection around the steady-state operating point. The identification method was validated with analytical solutions, which include the control system.

The identification method is based on the injection of low-amplitude sinusoids into the motor speed. The variation is small enough that the system can still be considered linear and time-invariant. Since the system is linear the same sinusoid frequency could be seen in the electromagnetic torque. The frequency is obtained with a discrete Fourier transform from both motor speed and electromagnetic torque. With this, the frequency response is constructed one frequency at a time.

The method was successfully implemented with the *motulator* simulation platform. A few key points were pointed out during the implementation. Moreover, the method was validated with one induction motor, which was controlled with three different control methods. Even more important is that the method works with multiple different control methods.

Future improvements on this topic could include reducing calculation time by using various input signals such as a pseudo-random binary sequence, maximum length binary sequence, and impulse response. The motor models could be improved by including multiple rotor branches, this could increase the accuracy [22]. Another topic could be an application program interface for the control system.

References

[1] IEA, *World Energy Outlook 2017*. Paris : OECD/IEA, 2017, [Online: https://iea.blob.core.windows.net/assets/4a50d774-5e8c-457e-bcc9-513357f9b2fb/World_Energy_Outlook_2017.pdf].

[2] M. I. Friswell, J. E. T. Penny, S. D. Garvey, and A. W. Lees, *Dynamics of Rotating Machines*. Cambridge University Press, 2010.

[3] C. A. Nickle and C. A. Pierce, "Stability of synchronous machines effect of armature circuit resistance," *Transactions of the American Institute of Electrical Engineers*, vol. 49, no. 1, pp. 338–350, 1930.

[4] I. M. Canay, "A Novel Approach to the Torsional Interaction and Electrical Damping of the Synchronous Machine. Part I: Theory," *IEEE Power Engineering Review*, vol. PER-2, no. 10, pp. 24–24, 1982.

[5] ——, "A Novel Approach to the Torsional Interaction and Electrical Damping of the Synchronous Machine. Part II," *IEEE Power Engineering Review*, vol. PER-2, no. 10, pp. 25–25, 1982.

[6] A. Tabesh and R. Iravani, "On the application of the complex torque coefficients method to the analysis of torsional dynamics," *IEEE Transactions on Energy Conversion*, vol. 20, no. 2, pp. 268–275, 2005.

[7] T. Holopainen, A.-K. Repo, and J. Järvinen, "Electromechanical interaction in torsional vibrations of drive train systems including an electrical machine," in *Proceedings of the 8th IFToMM International Conference on Rotordynamics*, Seoul, Korea, September 2010, pp. 933–940.

[8] G.-J. Jo and J.-W. Choi, "Rotor field-oriented v/ f drive system implementation with oscillation suppression compensator in induction motors," *IEEE Journal of Emerging and Selected Topics in Power Electronics*, vol. 9, no. 3, pp. 2745–2758, 2021.

[9] M. Hinkkanen, L. Tiitinen, E. Mölsä, and L. Harnefors, "On the stability of volts-per-hertz control for induction motors," *IEEE Journal of Emerging and Selected Topics in Power Electronics*, vol. 10, no. 2, pp. 1609–1618, 2022.

[10] L. Tiitinen, M. Hinkkanen, and L. Harnefors, "Stable and passive observer-based v/hz control for induction motors," in *2022 IEEE Energy Conversion Congress and Exposition (ECCE)*, Detroit, MI, USA, October 2022, pp. 1–8.

[11] G. F. Franklin, J. D. Powell, and A. Emami-Naeini, *Feedback control of Dynamic Systems*, 7th ed. Pearson, 2015.

[12] S. Skogestad and I. Postlethwaite, *Multivariable feedback control analysis and design*, 1st ed. Wiley, 1996.

[13] T. Holopainen and A. Arkkio, "Simple electromagnetic motor model for torsional analysis of variable speed drives with an induction motor," in *Technische Mechanik*, vol. 37, 2017, pp. 347–357.

[14] Y. Yi, D. Qin, and C. Liu, "Investigation of electromechanical coupling vibration characteristics of an rlectric drive multistage gear system," *Mechanism and Machine Theory*, vol. 121, pp. 446–459, 2018.

[15] L. Ljung, *System Identification: Theory for the User*, 2nd ed. Prentice-Hall, 1999.

[16] J. G. Proakis and D. G. Manolakis, *Digital Signal Processing*, 4th ed. Pearson, 2006.

[17] W. C. Duesterhoeft, M. W. Schulz, and E. Clarke, "Determination of instantaneous currents and voltages by means of alpha, beta, and zero components," *Transactions of the American Institute of Electrical Engineers*, vol. 70, no. 2, pp. 1248–1255, 1951.

[18] J. Pyrhönen, T. Jokinen, and V. Hrabovcová, *Design of rotating electrical machines*. Chichester, West Sussex, United Kingdom: Wiley, 2014.

[19] G. Slemon, "Modelling of induction machines for electric drives," *IEEE Transactions on Industry Applications*, vol. 25, no. 6, pp. 1126–1131, 1989.

[20] Aalto Electric Drives, *motulator: motor drive simulator in python*, Accessed 16 June 2022. [Online]. Available: https://github.com/Aalto-Electric-Drives/motulator

[21] Python Core Team, *Python: a dynamic, open source programming language*, Python Software Foundation, 2019, Python version 3.9, Accessed 16 August 2022. [Online]. Available: https://www.python.org/

[22] A. Arkkio and T. P. Holopainen, "Space-vector models for torsional vibration of cage induction motors," *IEEE Transactions on Industry Applications*, vol. 52, no. 4, pp. 2988–2995, 2016.